

Non-locality of Two Ultracold Trapped Atoms

Thomás Fogarty and Thomas Busch

Department of Physics, University College Cork, Cork, Republic of Ireland

John Goold

Centre for Quantum Technologies, National University of Singapore, 3 Science Drive 2, 117543, Singapore

Mauro Paternostro

School of Mathematics and Physics, Queen's University Belfast, Belfast, BT7 1NN, United Kingdom

Abstract. We undertake a detailed analysis of the non-locality properties of the fundamental problem of two trapped, distinguishable neutral atoms undergoing s-wave scattering. We show that this interaction generates continuous variable (CV) entanglement between the external degrees of freedom of the atoms and consider its behaviour as a function of both, the distance between the particles and the strength of the inter-particle scattering length. We first quantify the entanglement in the ground state of the system at zero temperature and then, adopting a phase-space approach, test the violation of the Clauser-Horn-Shimony-Holt inequality at both zero and non-zero temperature and under the effects of general dissipative local environments.

PACS numbers: 32.80.Pj, 05.30.Jp, 03.65.Ge, 03.67.Mn

1. Introduction

Ultracold atoms have recently emerged as ideal systems for the exploration of fundamental effects in quantum mechanics, quantum information and quantum simulation [1]. While a large amount of attention so far has been directed towards the exploitation of entanglement in the internal degrees of freedom of the atomic systems, the exploration of the external degrees of freedom as valuable physical supports for the encoding of continuous variables (CV) quantum information has not been considered extensively. This may have been motivated, arguably, by the difficulties faced so far in achieving a strong enough interaction between neutral, atomic CVs. However, it is by today experimentally possible to greatly enhance such coupling by, for example, driving Feshbach resonances using external magnetic fields [2]. Furthermore, techniques to trap, cool and control single neutral atoms have improved to an extent that high-fidelity measurements on single quantum particles are now possible [3, 4, 5]. For neutral atoms, optical lattices and dipole traps have been used in proposals for the implementation of fundamental two qubit gates [6, 7, 8]. Moreover, the flexibility typical of optical potentials allows one to consider spin dependent configurations [9]. Another example of the flexibility of such potentials is the ability to shape the trapping geometry in different spatial directions such that the dynamics of the system along one or several directions can be inhibited. For one-dimensional configurations, interactions can also be significantly enhanced through the so-called confinement-induced resonance [10].

With all this in mind, we will in the following investigate the entanglement generated among external degrees of freedom in the presence of enhanced inter-atomic couplings. For this we study an analytic, one-dimensional model of two atoms in separate harmonic traps which interact via a pseudopotential [11]. This model is an extension of the problem of two atoms interacting in a single harmonic trap [12], and its analytical solution was recently given in [18, 20]. One-dimensional models have recently shown to be in good agreement with experimental results [13], and the existence of analytical solutions has made them a good model to be used as a testbed for realistic studies of various facets of entanglement [14, 15, 16, 17].

Here we extend these works and investigate the non-local nature of the CV atomic state generated by the interaction using a phase-space-based version of Clauser-Horne-Shimony-Holt (CHSH) inequality derived in Ref. [19]. The analyticity of our model allows us to extend the study to finite temperature and take losses into account in an exact way, thus providing a full-comprehensive theoretical characterization of non-classical correlations within our system and paving the way to its experimental demonstration.

The presentation of the work is organised as follows. In Sec. 2 we introduce the system, briefly review its exact solution and quantify the degree of entanglement for its ground state using the von-Neumann entropy. In Sec. 3 we calculate the Wigner function of the atomic state and show that it has a considerable negative part, which is a strong indication of inherent non-classicality. In Sec. 4 we test for this non-locality by

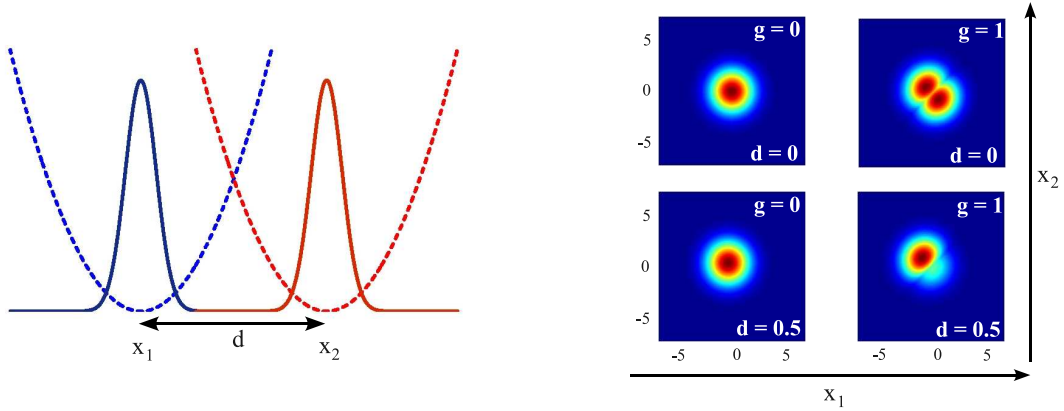


Figure 1. Panel (a) shows a pictorial representation of the model Hamiltonian Eq. 2. Panel (b) shows the two-particle probability density for two different values of distance d and interaction strength g .

calculating a continuous variable CHSH-like function [19] and discuss and illustrate the violation of local realistic theories for a wide range of parameters. In order to connect the results to experiments we extend our study to include the effects of a general dissipative environment in Sec. 5. Finally, Sec. 6 draws our conclusions and accesses the impact of our work.

2. Model Hamiltonian

The model we consider consists of two bosonic atoms confined along the x axis (the *axial direction*) with two separate, but overlapping harmonic potentials, as shown in Fig. 1(a). The atoms are tightly confined along directions perpendicular to x (the *transverse directions*) by high-frequency trapping potentials. As a result of the large energy level separation associated with the transverse eigenstates, at low temperature the transverse motion is restricted to the lowest mode. The system can then be described by the quasi one-dimensional Hamiltonian

$$\hat{H} = -\frac{\hbar^2}{2m_1}\nabla_1^2 - \frac{\hbar^2}{2m_2}\nabla_2^2 + \frac{m_1}{2}\omega^2(x_1 - d_1)^2 + \frac{m_2}{2}\omega^2(x_2 - d_2)^2 + g_{1D}\delta(x_1 - x_2), \quad (1)$$

where m_1 and m_2 are the masses of the two atoms and x_1 and x_2 are the respective spatial coordinates. We assume both traps to have the same frequency ω and be displaced by the distances d_1 and d_2 from the origin of the coordinate system. We model the atomic interaction using the standard point-like pseudo-potential and restrict ourselves to s-wave scattering. At low temperatures the scattering strength is then known to be given by $g_{1D} = -2\hbar^2/ma_{1D}$, where $m=m_1m_2/(m_1+m_2)$ is the reduced atomic mass and a_{1D} is the one-dimensional scattering length related to the actual three-dimensional one via $a_{1D} = -d_\perp^2/2a_{3D}(1 - Ca_{3D}/d_\perp)$. Here d_\perp is the size of the single-atom ground state

wavefunction in the transversal direction and $C \simeq 1.4603\dots$ is a constant [10]. By introducing the centre of mass coordinate $X = (x_1 + x_2)/2$ and the relative coordinate $x = (x_1 - x_2)/2$, the two-atom wavefunction can be factorised into $\phi(X)\psi(x)$ with $\phi(X)$ [$\psi(x)$] being the wavefunction for the centre-of-mass [relative motion] dynamics. Correspondingly, the Schrödinger equation decouples as

$$\left(-\frac{\hbar^2}{2M}\frac{\partial^2}{\partial X^2} + \frac{1}{2}M\omega^2 X^2\right)\phi(X) = \hbar\omega\left(n + \frac{1}{2}\right)\phi(X), \quad (2)$$

$$\left(-\frac{\hbar^2}{2m}\frac{\partial^2}{\partial x^2} + \frac{1}{2}m\omega^2(x-d)^2 + g_{1D}\delta(x)\right)\psi(x) = \hbar\omega\left(\nu + \frac{1}{2}\right)\psi(x), \quad (3)$$

where $d = d_1 - d_2$ and $M = 2m$. Clearly, the centre-of-mass dynamics has the form of simple harmonic motion while the relative problem consists of a displaced harmonic oscillator subjected to a point-like disturbance at position x .

For completeness sake we will in the following briefly sketch the steps required to solve eq. (3). Our approach follows the detailed treatment given in Refs. [18, 20]. We first scale all the involved lengths in units of $a = \sqrt{\hbar/2m\omega}$, which is the width of the ground state wavefunction along the axial direction, while the characteristic energies are rescaled in units of the energy of the unperturbed harmonic oscillator, $\hbar\omega$. Eq. (3) thus becomes (for $x \neq 0$)

$$\frac{d^2\psi}{d\xi^2} + \left(\nu + \frac{1}{2} - \frac{\xi^2}{4} - g\delta(\xi + d)\right)\psi = 0, \quad (4)$$

where $g = g_{1D}a/(\hbar\omega)$ is the renormalised strength of the δ -barrier, $\xi = (x-d)$ is a shifted spatial coordinate and we have dropped the spatial dependence of ψ for convenience. The solutions to this equation can be given in terms of parabolic cylinder functions, $D_\nu(\pm\xi)$, of order ν as follows

$$\psi_l = N_l D_\nu(-\xi) \quad \text{for } x < 0, \quad (5)$$

$$\psi_r = N_r D_\nu(\xi) \quad \text{for } x > 0, \quad (6)$$

where N_l and N_r are the normalization factors that can be calculated by imposing continuity of the solutions at the position of the δ -function. Explicitly, this leads to the following conditions

$$\frac{1}{2}\nu [D_{\nu-1}(-d)D_\nu(d) + D_{\nu-1}(d)D_\nu(-d)] - gD_\nu(-d)D_\nu(d) = 0, \quad (7)$$

for non-zero value at the position of the δ -function and

$$N_+\nu D_{\nu-1}(-d) + N_-\nu D_{\nu-1}(d) = 0, \quad (8)$$

whenever the functions are zero at the δ -function. This also determines the energy spectrum of the system which exhibits trap-induced shape resonances due to energy-level repulsion [18, 20]. The ground-state wavefunction can now be obtained as $\Psi_0(x_1, x_2) = \phi(X)\psi(x)$ and on the right-hand side of Fig. 1 we show the two particle probability density of the ground state, $|\Psi_0(x_1, x_2)|^2$. The repulsive interaction between the particles is evident as a zero line along the diagonal in the probability density when $x_1 = x_2$. For a finite trap separation the particles become localised in their respective

traps and the two particle probability density moves to occupy the upper left-hand side quadrant.

From this ground state we are able to explore the zero-temperature quantum correlations of the system by using the von Neumann entropy S of the reduced single-particle density matrix $\rho_1(x, x')$, which is determined as the kernel of the reduced density operator in configuration space

$$\rho_1(x, x') = \int_{-\infty}^{\infty} \Psi_0(x, x_2) \Psi_0^*(x', x_2) dx_2. \quad (9)$$

In order to evaluate S we need the eigenvalues λ_i of $\rho_1(x, x')$, which are found by numerically solving the integral-value equation

$$\int_{-\infty}^{+\infty} \rho_1(x, x') \psi_i(x') dx' = \lambda_i \psi_i(x), \quad (10)$$

where the $\psi_i(x)$ are the eigenstates associated with the λ_i . The von Neumann entropy is then calculated as $S = -\sum_i \lambda_i \log_2 \lambda_i$,

In Fig. 2 we show the von Neumann entropy as a function of both the trap distance d and the interaction strength g . For the case of a repulsive interaction it can be seen from Fig. 2(a) that the von Neumann entropy decreases with increasing particle separation. This should be expected as the short range interaction becomes less important as d increases and the state of the system tends towards the product state of two non-interacting particles. Fig. 2(b) shows the behaviour of S as a function of the interaction strength, revealing that, after an initial raise, S saturates to an asymptotic value that decreases as d grows. This is again due to the short-range of the interaction potential: as the interaction is ineffective for large d , the steady value of S would be smaller for increasing values of the separation. For attractive interactions (*i.e.* $g < 0$) the situation is slightly different and local maxima and saddle points in S can be observed at certain values of the trap separation [see Figs. 2(c) and (d)]. These are due to the trap-induced shape resonances resulting from the bound ground state. Note that, for a given value of d , comparatively smaller values of g are required in the attractive-potential case than in the repulsive one in order to achieve large values of S .

3. Calculation of the Wigner function and assessment of its negativity

We will now investigate the non-classicality of the two-atom state in a much broader range of operative conditions, including finite temperature. For this, the main tool in our study will be the Wigner function [21] associated with the two-particle state. For the specific case at hand, the Wigner function depends on the position and momentum variables x_j and p_j ($j = 1, 2$) it is defined as [21]

$$W(x_1, p_1; x_2, p_2) = \int d\xi d\varsigma \frac{e^{-\frac{i}{\hbar} p_1 \xi - \frac{i}{\hbar} p_2 \varsigma}}{4\pi^2 \hbar^2} \rho\left(x_1 + \frac{\xi}{2}, x_2 + \frac{\varsigma}{2}, p_1 - \frac{\xi}{2}, p_2 - \frac{\varsigma}{2}\right). \quad (11)$$

By integrating out the momenta or positions one can calculate the marginal spatial or momentum distributions of the two particles, respectively. It is straightforward

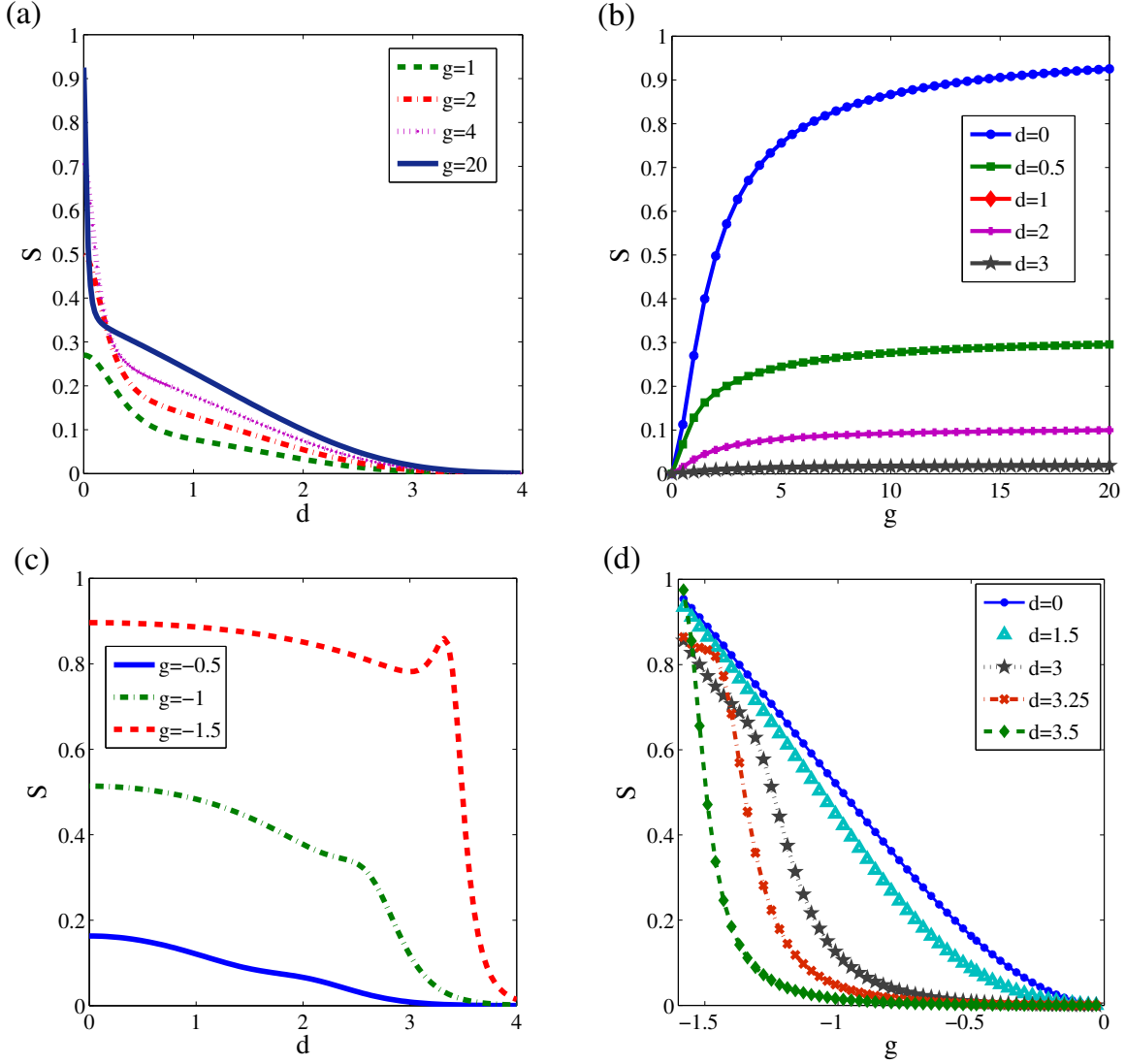


Figure 2. von Neumann entropy of the ground state for a repulsive interaction [panels (a) and (b)] and an attractive one [panels (c) and (d)]. Plots are shown for the von Neumann entropy versus trap separation, (a) and (c), and von Neumann entropy versus particle interaction strength, (b) and (d). The peaks present in (c) and (d) for certain values of d can be explained by the appearance of shape induced resonance in the energy spectrum.

to include the effects of a non-zero temperature by weighting the higher-order states of the two-atom spectrum with the appropriate Boltzmann factors, $P_{n,\sigma} = \frac{1}{\mathcal{Z}} e^{\frac{-E_{n,\sigma}}{k_B T}}$, where the $E_{n,\sigma}$ are the energies of the atomic eigenstates identified by the centre-of-mass and relative-motion quantum numbers n and σ , respectively. Moreover, we have introduced the equilibrium temperature of the system T , the Boltzmann constant k_B and the partition function \mathcal{Z} . We thus get

$$W(\alpha; \beta) = \sum_n \sum_{\sigma}^{\infty} P_{n,\sigma} W_{n,\sigma}(\alpha; \beta). \quad (12)$$

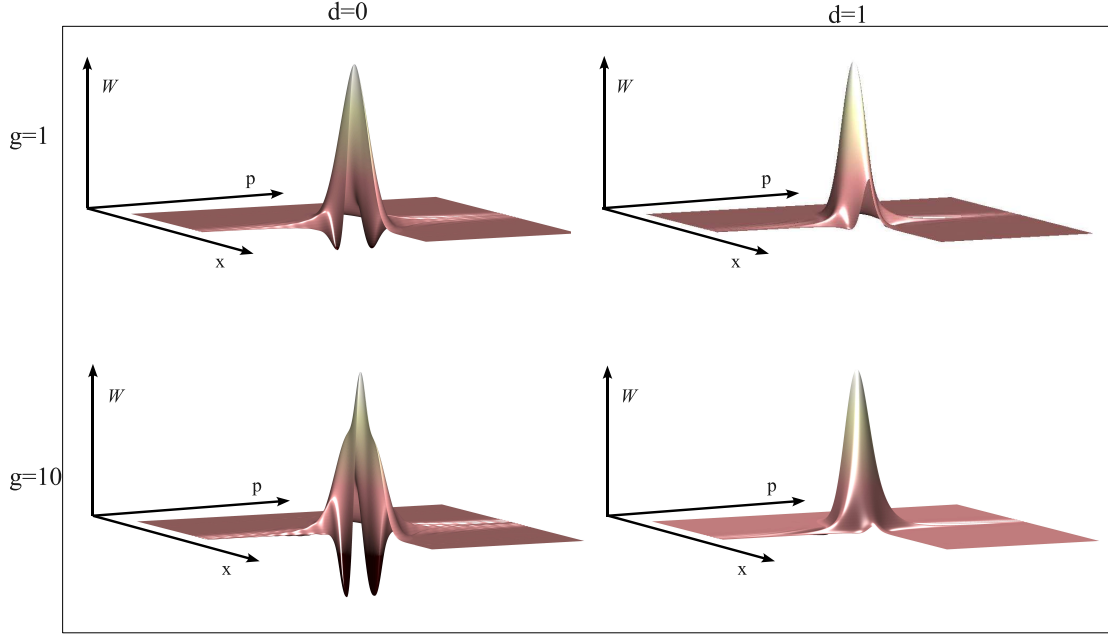


Figure 3. Wigner function for an interaction strength of $g = 1$ and $g = 10$ at interparticle distance $d = 0$ and $d = 1$. A quadrant is removed from the plot to show the negative parts of the Wigner distribution which is symmetric about $p = 0$. For $g = 1$ a reduction in the negative part of the Wigner function is evident for $d = 1$ compared to $d = 0$. For $g = 10$ the large negative contribution and sharp peak are indicative of the larger interaction strength at $d = 0$. For $d = 1$ the negative volume is significantly less.

For easiness of notation, we have written the Wigner function in terms of the two quadrature variable $\alpha = (x_1 + ip_1)/\sqrt{2}$ and $\beta = (x_2 + ip_2)/\sqrt{2}$. It is widely accepted that the appearance of negative values in the Wigner function of a system is a strong indication of non-classicality of the associated state. In fact, in this case $W(\alpha; \beta)$ cannot be interpreted as a classical probability distribution describing a microstate in the phase space. A good quantitative indicator for such non-classicality is the volume occupied by the negative regions of $W(\alpha; \beta)$ [22]. Note that as in our case the centre-of-mass part of the wavefunction does not depend on the interaction between the particles, it does not contribute to the degree of non-classicality.

In Fig. 3 we therefore show the Wigner functions associated with the relative part only for two different interaction strengths, g , and two distances between the particles, d . Negative parts are clearly visible for small values of d and become more prominent for increasing interaction strength. This is also visible in Fig. 4(a), where the volume of the negative part of the complete Wigner function, $W(\alpha; \beta)$, is plotted against d . However, the degree of non-classicality decreases faster for a larger interaction strength when the traps are moved apart. The temperature dependence of the negative volume is displayed in Fig. 4(b), where one can see a very fast decrease once the system is able to access states beyond the ground state.

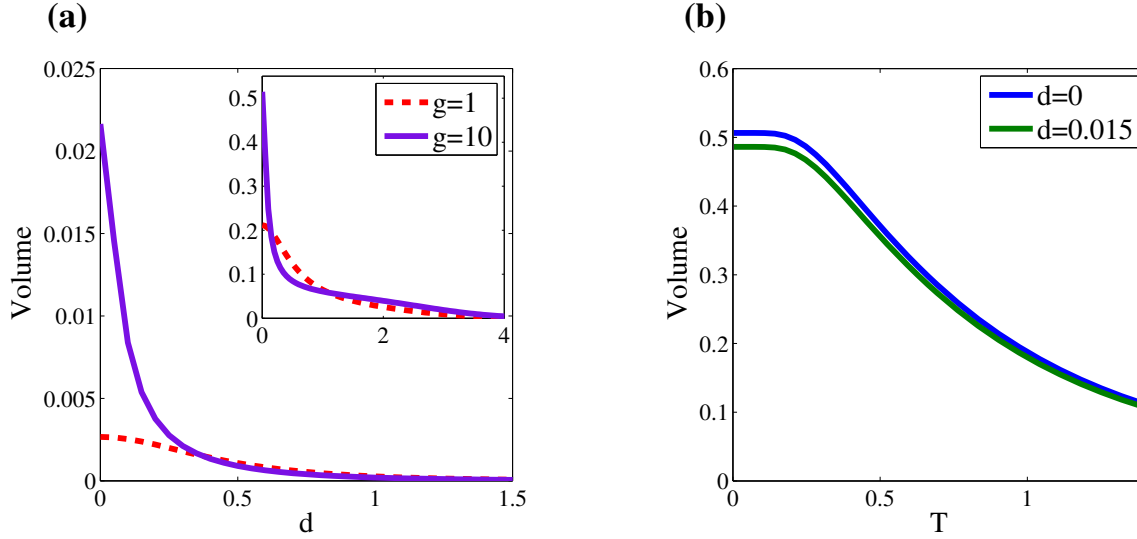


Figure 4. Panel (a) shows the negative volume of the complete Wigner distribution at zero temperature as a function of distance. The inset shows this value when only considering the relative part of the Wigner distribution. Panel (b) shows the negative volume with increasing temperature for the relative Wigner distribution with an interaction strength of $g=10$.

4. Testing non-locality in phase space

The results of the previous Section indicate that a considerable degree of non-classicality might be set in the state of the external degrees of freedom of the two trapped atoms, resilient to some extents to the effects of finite temperature. Moreover, as it should also be clear from Eq. (1), our study has shown the evident non-Gaussian nature of the atomic state (as witnessed by the features of the Wigner function). While correlations in Gaussian states are well and easily characterized, we face the lack of necessary and sufficient criteria for the quantification of entanglement in non-Gaussian states. In fact, the available entanglement measures for CV states are based (to the best of our knowledge) on the use of the negativity of partial transposition criterion formulated in terms of covariance matrices, which carry exact information on the state of a system only in the Gaussian scenario [23]. The lack of efficient ways to quantify entanglement makes an assessment of non-classicality in terms of non-locality very appealing and, basically, is the only rigorous way to ascertain whether or not a given non-Gaussian state is rightfully entangled or not.

We thus consider the CV version of CHSH inequality developed in Ref. [19] and will briefly remind the reader of the key points for completeness. It is well known that the Wigner function calculated at the origin of phase space is equivalent to the expectation value $W(\alpha = 0; \beta = 0) = \frac{4}{\pi^2} \langle \hat{\Pi}_1 \otimes \hat{\Pi}_2 \rangle$, where $\hat{\Pi}_j$ is the parity operator for mode $j = 1, 2$ [24]. The total Wigner function can therefore be written by using *displaced*

parity operators as [24]

$$W(\alpha; \beta) = \frac{4}{\pi^2} \langle \hat{D}_1(\alpha) \hat{\Pi}_1 \hat{D}_1^\dagger(\alpha) \otimes \hat{D}_2(\beta) \hat{\Pi}_2 \hat{D}_2^\dagger(\beta) \rangle, \quad (13)$$

where $\hat{D}_j(\alpha)$ is a displacement operator for mode j of amplitude α [23]. A CHSH-like function can thus be built starting from the above as

$$\mathcal{B} = \frac{\pi^2}{4} [W(0; 0) + W(\sqrt{\mathcal{J}}; 0) + W(0; -\sqrt{\mathcal{J}}) - W(\sqrt{\mathcal{J}}; -\sqrt{\mathcal{J}})] \quad (14)$$

with \mathcal{J} a positive constant. Local realistic theories impose $|\mathcal{B}| \leq 2$ [19] and any value outside this range indicates non-local behaviour.

Equipped with these tools, we can now quantitatively study the non-locality in the state of our system. Using the Wigner function calculated in Sec. 3, we determine the violation of the CHSH inequality optimised over \mathcal{J} and study the behaviour of \mathcal{B} against the interaction strength between the particles and the distance between the traps. In Fig. 5(a) we show the numerically optimised values of \mathcal{B} against d for various interaction strengths g and at zero temperature. Clearly, for short distances the violation of the local realistic bound is larger for strong interactions. The situation is somehow reverted at large distances, where weakly interacting atomic pairs appear to violate the CHSH inequality more significantly. Such an apparently counterintuitive result can be understood by reminding oneself that the one-dimensional interaction strength is inversely proportional to the one-dimensional scattering length (see Sec. 2): a lower value of g corresponds to a longer scattering length. Comparing these results to the von Neumann entropy shown in Fig. 2 it is evident that achieving a non-zero von Neumann entropy does not necessarily correspond to the violation of CHSH inequality. This point is in qualitative agreement with the findings of Ref. [14] and can be explained by the non-ideality of the above formulation for non-Gaussian states such as that of the two trapped atoms we are considering. It would be interesting to compare the behaviour found here with those corresponding to longer-range interaction potentials which might well lead to sustained non-locality at larger distances. In Fig. 5(b) we show \mathcal{B} as a function of the interaction strength. The non monotonic behaviour of the CHSH function against the interaction strength, as well as the disappearance of any violation at finite values of g and for $d \neq 0$, are striking. It can be understood by realising that the offset between the traps breaks the symmetry of the system and a large repulsive interaction between the particles results in less overlap and therefore less correlations in the phase space.

For the case of non-zero temperature we plot the violation of the CHSH inequality for two values of interaction strengths ($g = 1, 10$) in Fig. 5. While the similarity of the plots shows the general trends of decay of the correlations with increasing temperature and distance, one can note that for $g = 1$ the system is more resilient to the effects of an increasing temperature than in the stronger-interaction case because the separations between neighbouring energy levels increases at low δ -barrier (*i.e.* small g 's). At small g , this implies a greater probability to excite higher-energy modes at small temperature. Evidently, the violation of CHSH inequality becomes very sensitive to temperature variations once the thermal energy is comparable to the energy-level separation.

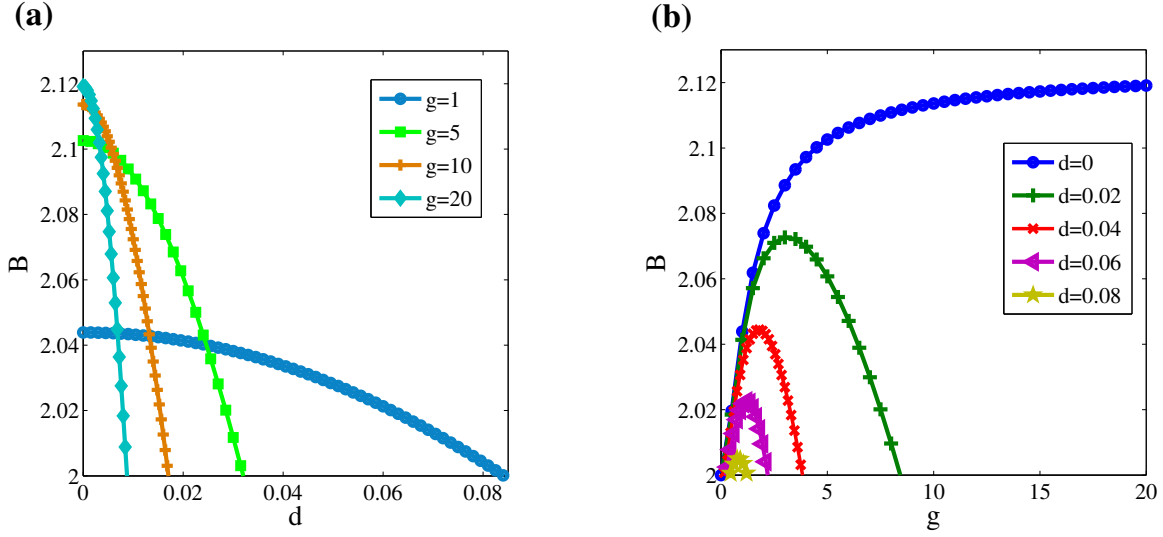


Figure 5. The violation of the CHSH inequality at $T = 0$ is shown in panel (a) against trap separation for various interaction strengths and in (b) versus g , for increasing trap separations.

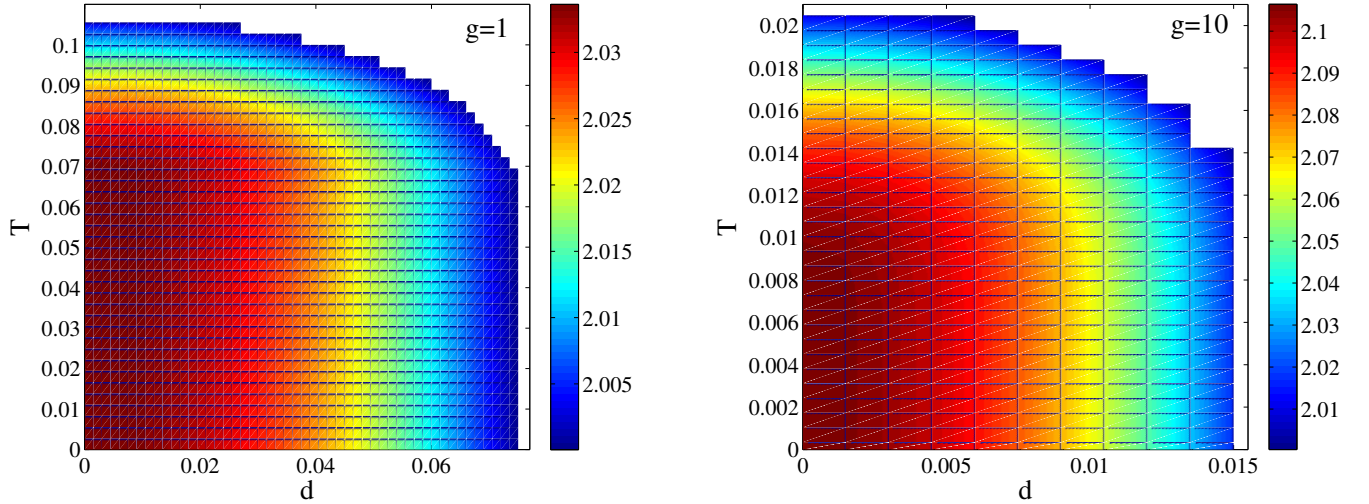


Figure 6. Degree of CHSH violation against particle-separation and temperature for interaction strengths of $g = 1$ and $g = 10$. The change in temperature has a greater impact on the two particles at greater interaction energies.

We conclude this Section by sketching a strategy to follow for the reconstruction of the atomic Wigner function for a non-locality test. The approach suggested by Lutterbach and Davidovich [25] is perfectly suited for our needs. The key is mapping the information encoded in the external degree of freedom of one of the trapped atoms into specific internal state of the atom itself, which can then be efficiently read out. For the sake of argument, let us for the moment address the case of a single atom and label the logical states of the qubit as $\{|\uparrow\rangle, |\downarrow\rangle\}$. Physically, they could be two quasi-degenerate

metastable ground states of a three-level Λ -like model. Guiding the transition from each ground state to the excited level of the Λ model, motional state-dependent sidebands are induced on $|\uparrow\rangle$ and $|\downarrow\rangle$. The transition between different motional states of the atom can thus be induced by properly tuned stimulated Raman passages connecting two different sidebands of the ground-state doublet, as described in [26], in a way so as to mimic the dynamics intertwining motional degrees of freedom and internal ones in trapped ions. Working in an appropriate Lamb-Dicke limit (where the recoil energy due to the *kicks* induced by the coupling between atomic levels and light is much smaller than the ground-state energy of the motional mode), it is possible to relate the difference $P_\uparrow - P_\downarrow$ between the probability of finding the atom in $|\uparrow\rangle$ or $|\downarrow\rangle$, respectively, to the expectation value of the displaced parity operator and thus, in turn, to the value of the Wigner function at a given point of the phase space [25]. Such a difference in probability can be effectively measured by means of routinely implemented high-efficiency fluorescence light-based detection methods [27]. In order to reconstruct the two-atom Wigner function, it would be sufficient to collect signals from both the atoms undergoing similar reconstruction protocols and appropriately putting together the statistical data gathered.

5. Effects of dissipation

Let us finally discuss the influence of a general loss mechanisms, one per atomic mode, that may affect the two-atom state due to finite-time coherence of the external degrees of freedom. Alternatively, our study could equivalently be used so as to take into account the effects of a finite-efficiency detection apparatus for the non-locality test (although fluorescence-based methods have very high efficiency, close to 100%, ideality of signal-collection is not yet achieved). Both models can be abstractly yet rigorously described by considering a simple *beam-splitter model* as follows: assuming low temperature environments allows us to describe them as two independent zero- T bosonic baths, each prepared in its collective vacuum state. We call A (B) the environmental bath affecting mode 1 (2). The Wigner function of the vacuum state of each is

$$W_0(\mu_k) = \frac{2}{\pi} e^{-2|\mu_k|^2} \quad (k = A, B), \quad (15)$$

where $\mu_k = \frac{x_k + ip_k}{\sqrt{2}}$ and x_k, p_k are the quadrature variables of the environmental modes. The interaction between the signal mode j and its environment is modelled as a mixing at a beam splitter having reflectivity η_k . For simplicity and without affecting the generality of our discussions, we assume the reflectivity to be equal in both modes, $\eta_k = \eta$. In phase space, the state of the signal mode after the interaction and after tracing over the environmental degrees of freedom is described by the convolution

$$W^\eta(x_1, x_2, p_1, p_2) = \int dx_A dx_B dp_A dp_B W(\tilde{x}_1, \tilde{p}_1, \tilde{x}_2, \tilde{p}_2) \\ \times W_0(\tilde{x}_A, \tilde{p}_A) W_0(\tilde{x}_B, \tilde{p}_B), \quad (16)$$

where we have introduced the transformed variables

$$\tilde{x}_j = \sqrt{\eta} x_j - \sqrt{1 - \eta} x_k, \quad \tilde{x}_k = \sqrt{\eta} x_k + \sqrt{1 - \eta} x_j, \quad (17)$$

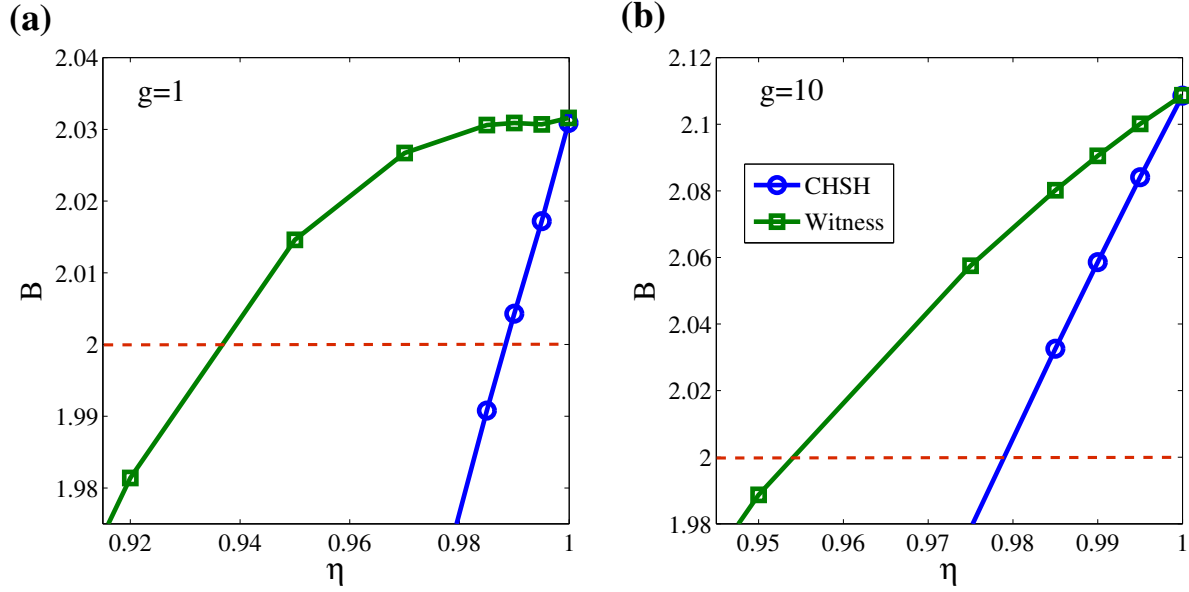


Figure 7. Plots of CHSH violation and entanglement witness for interaction strengths of $g = 1$ (panel (a)) and $g = 10$ (panel (b)) with inefficiency η . The violation of CHSH is seen to decay quickly as the detection becomes inefficient (blue lines), however the entanglement witness (green lines) shows the existence of entanglement for greater inefficiencies, with the lower value of g having more resilience to the losses.

$$\tilde{p}_j = \sqrt{\eta} p_j - \sqrt{1 - \eta} p_k, \quad \tilde{p}_k = \sqrt{\eta} p_k + \sqrt{1 - \eta} p_j \quad (18)$$

and one should take $k = A$ (B) if $j = 1$ (2). Eq. (16) is evaluated numerically and used to test violation of the CHSH inequality against η . Needless to say, the effect of losses (or detection inefficiencies) is to reduce the degree of violation of the CHSH inequality, as shown by the solid blue lines in Fig. 7. The same trend highlighted before regarding resilience of non-locality properties for lower values of g is somehow retrieved here.

It is therefore highly desirable to design viable strategies for a more robust analysis of non-locality. A step in this direction has been recently performed in Ref. [28] with the proposal of a robust entanglement witness based on a CHSH-like inequality that shows resilience with respect to losses/detection inefficiencies of the form considered here. Following the derivation provided by Lee *et al.* [28], one can see that for separable bipartite states and loss rate/detection inefficiency η , the following inequalities hold

$$\begin{aligned} |\langle \mathcal{W}_{\eta > \frac{1}{2}} \rangle| &= \left| \frac{\pi^2}{4\eta^2} [W^\eta(0, 0) + W^\eta(0, -\sqrt{\mathcal{J}}) + W^\eta(\sqrt{\mathcal{J}}, 0) - W^\eta(\sqrt{\mathcal{J}}, -\sqrt{\mathcal{J}})] \right. \\ &\quad \left. + \frac{\pi(\eta - 1)}{\eta^2} [W_\alpha^\eta(0) + W_\beta^\eta(0)] + 2(1 - \frac{1}{\eta})^2 \right| \leq 2, \\ |\langle \mathcal{W}_{\eta \leq \frac{1}{2}} \rangle| &= |\pi^2 [W^\eta(0, 0) + W^\eta(0, -\sqrt{\mathcal{J}}) + W^\eta(\sqrt{\mathcal{J}}, 0) - W^\eta(\sqrt{\mathcal{J}}, -\sqrt{\mathcal{J}})] \\ &\quad - 2\pi [W_1^\eta(0) + W_2^\eta(0)] + 2| \leq 2. \end{aligned} \quad (19)$$

Here, $W^\eta(a, b)$ is the two-mode Wigner function calculated in Eq. (16) and $W_{1,2}^\eta$ are its single-mode marginals. For the case of perfect detectors ($\eta = 1$) the inequality becomes

equivalent to (14). It is apparent that any violation of this inequality for $\eta < 1$ ensures the violation of the CHSH-inequality in the presence of the unitary case as well, thus such witness can be used effectively for detecting entanglement in the presence of noise. The results shown in Fig. 7 are that, while the CHSH inequality violation is lost for $\eta = 0.98$ at $g = 10$, the entanglement witness still violates it at $\simeq 0.95$, which is a small yet significant improvement. It is significant to notice that current avalanche photodiodes used to collect fluorescence have quantum efficiencies exactly in this range. Interestingly the entanglement witness for $g = 1$ is violated for smaller η , echoing the trend noticed for the CHSH at zero and non-zero temperature: lower interaction strengths give rise to states more resilient to influences from the environment.

6. Conclusions

We have investigated entanglement in a system of two interacting bosons in separate harmonic trapping potentials under a variety of conditions. The von Neumann entropy shows strong correlations at zero temperature and violation of local realistic theories for a wide range of relevant parameters. Interesting and rather counterintuitive behavior has been observed, even at non-zero temperature, for the whole range of interactions used. We have provided a clear interpretation for the multiple facets of both the revealed non-locality and the von Neumann entropy in terms of the details of the coupling model we have used and the spectrum of the system.

Finally, we have included the effects of general non-idealities (such as dissipative losses affecting the motional degrees of freedom of the trapped atoms or inefficient detection apparatuses), showing some fragility of the atomic non-locality. In order to circumvent such a hindrance, we have shown that some advantages can come from the use of a recently proposed entanglement witness that fits very well with the general approach put forward here. We hope that the realistic nature of our proposal, which although not immune from difficulties is a significant model to test non-classicality of massive systems and is by nature rather close to current state of the art, would spur experimental interest in the study of non-classical behaviour of simple low-dimensional atomic systems under non-ideal working conditions.

7. Acknowledgements

We acknowledge financial support from the Irish Research Council for Science and Engineering under the Embark initiative RS/2009/1082 and Science Foundation Ireland under grants no. 05/IN/I852 and 05/IN/I852 NS. JG would like to thank the National Research Foundation and Ministry of Education of Singapore for support and Mr. G. Vacanti for interesting discussions. MP is grateful to Dr. Seungwoo Lee and Prof. Hyunseok Jeong for invaluable comments and thanks the UK EPSRC for financial support (EP/G004579/1).

8. Bibliography

- [1] I. Bloch, J. Dalibard and W. Zwerger, *Rev. Mod. Phys.* **80**, 885 (2008).
- [2] C. Chin, R. Grimm, P. Julienne, *Rev. Mod. Phys.* **82**, 1225 (2010).
- [3] J. Beugnon, M. P. A. Jones, J. Dingjan, B. Darquié, G. Messin, A. Browaeys and P. Grangier, *Nature* **440**, 779 (2006).
- [4] M. Anderlini, P. J. Lee, B. L. Brown, J. Sebby-Strabley, W. D. Phillips and J. V. Porto, *Nature* **448**, 452 (2007).
- [5] T. Wilk, A. Gaëtan, C. Evellin, J. Wolters, Y. Miroshnychenko, P. Grangier and A. Browaeys, *Phys. Rev. Lett.* **104**, 010502 (2010).
- [6] D. Jaksch, H.-J. Briegel, J. I. Cirac, C. W. Gardiner, and P. Zoller, *Phys. Rev. Lett.* **82**, 1975 (1999).
- [7] T. Calarco, E. A. Hinds, D. Jaksch, J. Schmiedmayer, J. I. Cirac, and P. Zoller, *Phys. Rev. A* **61**, 022304 (2000).
- [8] L. Isenhower, E. Urban, X. L. Zhang, A. T. Gill, T. Henage, T. A. Johnson, T. G. Walker, and M. Saffman, *Phys. Rev. Lett.* **104**, 010503 (2010).
- [9] O. Mandel, M. Greiner, A. Widera, T. Rom, T.W. Hänsch and I. Bloch, *Phys. Rev. Lett.* **91**, 010407 (2003)
- [10] M. Olshanii, *Phys. Rev. Lett.* **81**, 938 (1998).
- [11] K. Huang and C. N. Yang, *Phys. Rev.* **105**, 767 (1957).
- [12] Th. Busch, B. G. Englert, K. Rzazewski, and M. Wilkens, *Found. Phys.* **28**, 549 (1998).
- [13] T. Stöferle, H. Moritz, K. Gönter, M. Köhl and T. Esslinger, *Phys. Rev. Lett.* **96**, 030401 (2006).
- [14] H. Mack and M. Freyberger, *Phys. Rev. A* **66**, 042113 (2002).
- [15] B. Sun, D. Zhou and L. You, *Phys. Rev. A* **73**, 012336 (2006).
- [16] D. S. Murphy, J. F. McCann, J. Goold, and Th. Busch, *Phys. Rev. A* **76**, 053616 (2007).
- [17] J. Goold, L. Heaney, Th. Busch, and V. Vedral *Phys. Rev. A* **80**, 022338 (2009).
- [18] M. Krych and Z. Idziaszek, *Phys. Rev. A* **80**, 022710 (2009).
- [19] K. Banaszek and K. Wodkiewicz, *Phys. Rev. A* **58**, 4345 (1998); *Phys. Rev. Lett.* **82** 2009 (1999).
- [20] J. Goold, M. Krych, T. Fogarty, Z. Idziaszek and Th. Busch, <http://arxiv.org/abs/1006.0198>
- [21] E. P. Wigner, *Phys. Rev* **40**, 749 (1932).
- [22] A. Kenfack and K. Życzkowski, *J. Opt. B: Quantum Semiclass. Opt.* **6**, 396 (2004).
- [23] S. L. Braunstein and P. van Loock, *Rev. Mod. Phys.* **77**, 513 (2005).
- [24] A. Royer, *Phys. Rev. A* **15**, 449 (1977).
- [25] L. G. Lutterbach and L. Davidovich, *Phys. Rev. Lett.* **78**, 2547 (1997).
- [26] A. S. Parkins and E. Larsabal, *Phys. Rev. A* **63**, 012304 (2000); M. Paternostro, M. S. Kim, and P. L. Knight, *Phys. Rev. A* **71**, 022311 (2005).
- [27] C. Monroe *et al.*, *Science* **272**, 1131 (1996).
- [28] S. W. Lee, H. Jeong and D. Jaksch, *Phys. Rev. A* **81**, 012302 (2010).